The Planar Circuit—An Approach to Microwave Integrated Circuitry

TAKANORI OKOSHI, MEMBER, IEEE, AND TANROKU MIYOSHI, STUDENT MEMBER, IEEE

Abstract—Three principal categories have been known in electrical circuitry so far. They are the lumped-constant (0-dimensional) circuit, distributed-constant (1-dimensional) circuit, and waveguide (3-dimensional) circuit. The planar circuit to be discussed in general in this paper is a circuit category that should be positioned as a 2-dimensional circuit. It is defined as an "electrical circuit having dimensions comparable to the wavelength in two directions, but much less thickness in one direction."

The main subject of this paper is the computer analysis of an arbitrarily shaped, triplate planar circuit. It is shown that a computer analysis based upon a contour-integral solution of the wave equation offers an accurate and efficient tool in the design of the planar circuit. Results of some computer calculations are described.

It is also shown that the circuit parameters can be derived directly from Green's function of the wave equation when the shape of the circuit is relatively simple. Examples of this sort of analysis are also shown for comparison with the computer analysis.

I. Introduction

THREE PRINCIPAL categories have been known in electrical circuitry so far. They are the lumped-constant (0-dimensional) circuit, distributed-constant (1-dimensional) circuit, and waveguide (3-dimensional) circuit. The planar circuit to be discussed in general in this paper is a circuit category that should be positioned as a 2-dimensional circuit. It is defined as an "electrical circuit having dimensions comparable to the wavelength in two directions, but much less thickness in one direction."

Then three types of the planar circuit are possible. They are the triplate type, the open type, and the cavity type, as shown in Fig. 1. However, in this paper mainly the triplate-type planar circuit will be dealt with to avoid confusion.

There are three reasons that the planar circuit should be investigated in general at present [1], [2].

1) The planar circuit has wider freedom in the circuit design than the stripline circuit does. In other words, the former includes the latter as a special case. Therefore, if the design technique for the planar circuit is established in future, it will offer an exact and efficient tool in the design of microwave integrated circuits.

2) The planar circuit can offer a lower impedance level than the stripline circuit does. The recently developed microwave semiconductor devices, such as Gunn, IMPATT, or Schottky-barrier diodes, usually require a low-impedance circuitry.

Manuscript received March 10, 1971; revised September 7, 1971.
The authors are with the Department of Electronic Engineering, University of Tokyo, Tokyo, Japan.

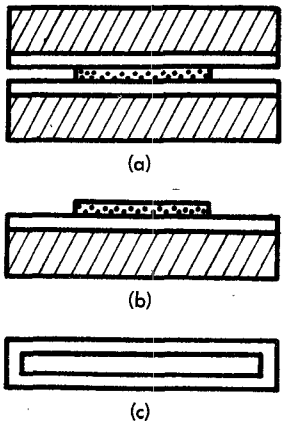

Fig. 1. Three types of the planar circuit. (a) Triplate type. (b) Open type. (c) Cavity type.

3) The planar circuit is easier to analyze and design than the waveguide circuit. By virtue of the recent progress in the computer, the analysis of an arbitrarily shaped planar circuit is within our reach if we rely on the computer.

We should note that the planar circuit is not an entirely new concept. A special case of this circuitry, the disk-shaped resonator, has been used in the stripline circulator or even as a filter [3]–[5]. The so-called "radial line" is also a special case of the planar circuit. However, to the authors' knowledge, general treatment of the planar circuit, or, in other words, the analysis of an arbitrarily shaped planar circuit, has never been presented.

The main subject of this paper is the analysis of an arbitrarily shaped, triplate planar circuit. The term "analysis" denotes here the determination of the circuit parameters of the equivalent multiport as shown in Fig. 2.

II. Basic Equations

A symmetrically excited, triplate planar circuit as shown in Fig. 2(a) will be considered throughout this paper. The model to be considered is as follows.

An arbitarily shaped, thin conductor plate is sandwiched between two ground conductors, with a spacing d from each of them. The circuit is assumed to be excited symmetrically with respect to the upper and lower ground conductors. There are several coupling ports, and their widths are denoted by W_i, W_j, $\cdots$. The rest of the periphery is assumed to be open circuited. The

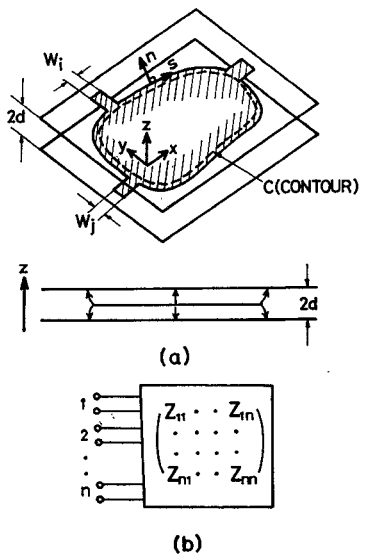

Fig. 2. (a) An arbitrarily shaped planar circuit. (b) Its equivalent multiport circuit.

xy coordinates and the z axis, respectively, are set parallel and perpendicular to the conductors.

When the spacing d is much smaller than the wavelength and the spacing material is homogeneous and isotropic, it is deduced directly from Maxwell's equation that a two-dimensional Helmholtz equation dominates the electromagnetic field in the planar circuit:

$$(\nabla_T^2 + k^2)V = 0, \qquad k^2 = \omega^2\epsilon\mu, \quad \nabla_T^2 = \frac{\partial^2}{\partial x^2} + \frac{\partial^2}{\partial y^2} \tag{1}$$

where V denotes the RF voltage of the center conductor with respect to the ground conductors; ω, ϵ, and μ are the angular frequency, permittivity, and permeability of the spacing material, respectively.[1] The network characteristics can be determined by solving (1) under given boundary conditions.

At most of the periphery where the coupling ports are absent, no current flows at the edge of the center conductor in the direction normal to the edge, because the circuit is excited symmetrically with respect to the upper and lower ground conductors.[2] Hence, the following boundary condition must hold:

$$\partial V/\partial n = 0 \tag{2}$$

where n is normal.

[1] In most of the discussions in this paper the circuit is assumed to be lossless. When we consider a small circuit dissipation, k is given, approximately, as

$$k = k' - jk'', \qquad k' \gg k'' \tag{F1}$$

where

$$k' = \omega\sqrt{\epsilon\mu}$$

$$k'' = \omega\sqrt{\epsilon\mu}\,(\tan\delta + r/d)/2 \tag{F2}$$

δ is loss angle of the spacing material, and r is skin depth.

[2] This is equivalent to assuming that the periphery is a perfect magnetic wall. Actually, however, a fringing field [see Fig. 2(a)] is always present. A simple but reasonable correction for it is to extend the periphery outwards by $2d(\log_e 2)/\pi$ to simulate the *static* fringing capacitance.

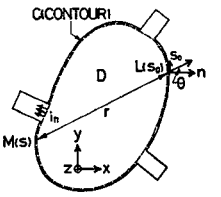

Fig. 3. Symbols used in the integral equation.

At a coupling port, (2) is no longer valid. Let the width of the port and the surface current density normal to the periphery C be denoted by W and i_n, respectively. If an admittance Y is connected to this port,

$$Y \doteqdot \frac{2\int_W i_n ds}{\int_W V ds/W} = \frac{-2jW\int_W \left(\frac{\partial V}{\partial n}\right) ds}{\omega\mu d\int_W V ds} \tag{3}$$

holds. The factor 2 expresses the fact that the current flows on both the upper and lower surfaces of the center conductor.

III. Computer Analysis

A. Integral Equation

The main feature of the planar circuit, as compared with waveguide circuit, is that we can analyze an arbitrarily shaped planar circuit within a reasonable computer time.

We consider an arbitrarily shaped, triplate planar circuit with several coupling ports, as shown in Fig. 3. Solving the wave equation over the entire area inside the contour C will require a long computer time. However, when we are concerned only with the RF voltage along the periphery, such a computation is not necessary. Using Weber's solution for cylindrical waves [6], the potential at a point upon the periphery is found to satisfy the following equation (refer to the Appendix for the detail of the derivation):

$$2jV(s) = \oint_c \{k\cos\theta H_1^{(2)}(kr)V(s_0) - j\omega\mu d\, i_n(s_0)H_0^{(2)}(kr)\}ds_0. \tag{4}$$

In this equation $H_0^{(2)}$ and $H_1^{(2)}$ are the zeroth-order and first-order Hankel functions of the second kind, respectively, i_n denotes the current density flowing outwards along the periphery, s and s_0 denote the distance along contour C. The variable r denotes distance between points M and L represented by s and s_0, respectively, and θ denotes the angle made by the straight line from point M to point L and the normal at point L, as shown in Fig. 3. When i_n is given, (4) is a second-kind Fredholm equation in terms of the RF voltage.

B. Circuit Parameters of an Equivalent N-Port [7]

For numerical calculation we divide the periphery into N incremental sections numbered as 1, 2, · · · , N,

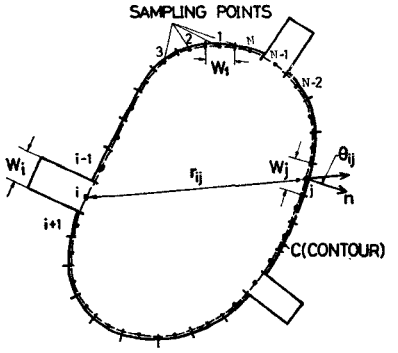

Fig. 4. Symbols used in the computer analysis.

having widths $W_1, W_2, \cdots, W_N$, respectively, as illustrated in Fig. 4. Coupling ports are assumed to occupy each one of those sections. Further, we set N sampling points at the center of each section.

When we assume that the magnetic and electric field intensities are constant over each width of those sections, the above integral equation results in a matrix equation:

$$2jV_i = \sum_{j=1}^{N} \{kV_jG_{ij} + j\omega\mu dI_jF_{ij}\} \tag{5}$$

where

$$F_{ij} = \begin{cases} \dfrac{1}{W_j}\displaystyle\int_{W_j} H_0^{(2)}(kr)ds, & (i \neq j) \\ 1 - \dfrac{2j}{\pi}\left(\log\dfrac{kW_i}{4} - 1 + \gamma\right), & (i = j) \end{cases}$$

$$G_{ij} = \begin{cases} \displaystyle\int_{W_j} \cos\theta H_1^{(2)}(kr)ds, & (i \neq j) \\ 0, & (i = j) \end{cases} \tag{6}$$

$\gamma = 0.5772 \cdots$ is Euler's constant, and $I_j = -i_nW_j$ represents the total current flowing into the jth port. The formulas for F_{ii} and G_{ii} in (6) have been derived assuming that the ith section is straight.

We can temporarily consider that all the N sections upon the periphery are coupling ports and that the planar circuit is represented by an N-port equivalent circuit. Then, from the above relations, the impedance matrix of the equivalent N-port circuit is obtained as

$$Z = U^{-1}H \tag{7}$$

where U and H denote N-by-N matrices determined by the shape of the circuit, whose components are given as

$$\begin{cases} u_{ij} = -kG_{ij}, & (i \neq j) \\ u_{ii} = 2j \end{cases} \qquad h_{ij} = j\frac{\omega\mu d}{2}F_{ij} \tag{8}$$

and U^{-1} denotes the inverse matrix to U.

In practice, most of the N ports described above are open circuited. When external admittances are connected to several of them and the rest of the ports are left open circuited, the reduced impedance matrix can be derived without difficulty.

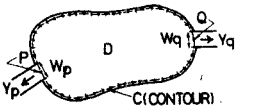

Fig. 5. Center conductor of a two-port planar circuit.

C. Transfer Parameters of a Two-Port Circuit [8]

In the case of a two-port circuit, the transfer parameters A, B, C, and D of the equivalent two-port can be given more simply as follows.

Suppose P and Q denote the driving terminal and load terminal, respectively, as shown in Fig. 5. Admittances Y_p and Y_q are connected to those terminals:

$$Y_p = 2i_n(P)W_p/V_p$$
$$Y_q = 2i_n(Q)W_q/V_q. \tag{9}$$

Then Y_p has a negative conductance component. Equation (5) can be applied to all the N sampling points. Thus the RF voltage at each point can be given by the following matrix equation:

$$[U + Y_pV + Y_qW]\begin{bmatrix} V_1 \\ \cdot \\ \cdot \\ V_N \end{bmatrix} = 0 \tag{10}$$

where V and W are again matrices determined by the shape of the circuit:

$$V = \begin{bmatrix} 0 & \cdot & \overset{p}{v_{1p}} & \cdot & 0 \\ \cdot & \cdot & \cdot & \cdot & \cdot \\ \cdot & \cdot & \cdot & \cdot & \cdot \\ 0 & \cdot & v_{Np} & \cdot & 0 \end{bmatrix}, \qquad v_{ip} = h_{ip}$$

$$W = \begin{bmatrix} 0 & \cdot & \overset{q}{w_{1q}} & \cdot & 0 \\ \cdot & \cdot & \cdot & \cdot & \cdot \\ \cdot & \cdot & \cdot & \cdot & \cdot \\ 0 & \cdot & w_{Nq} & \cdot & 0 \end{bmatrix}, \qquad w_{iq} = h_{iq}.$$

In order that a steady field exists in the circuit, from the nontrivial condition,

$$\det [U + Y_pV + Y_qW] = 0 \tag{11}$$

must hold. This equation directly gives a bilinear relation between $-Y_p$, the driving point admittance, and Y_q, the load admittance, as

$$-Y_p = \frac{C' + D'Y_q}{A' + B'Y_q} \tag{12}$$

where A', B', C', and D' are given as the following de-

terminants:

$$A' = \begin{vmatrix} u_{11} & \cdots & \overset{p}{v_{1p}} & \cdots & u_{1N} \\ \cdot & \cdots & \cdot & \cdots & \cdot \\ \cdot & \cdots & \cdot & \cdots & \cdot \\ u_{N1} & \cdots & v_{Np} & \cdots & u_{NN} \end{vmatrix}$$

$$B' = \begin{vmatrix} u_{11} & \cdots & \overset{p}{v_{1p}} & \cdots & \overset{q}{w_{1q}} & \cdots & u_{1N} \\ \cdot & \cdots & \cdot & \cdots & \cdot & \cdots & \cdot \\ \cdot & \cdots & \cdot & \cdots & \cdot & \cdots & \cdot \\ u_{N1} & \cdots & v_{Np} & \cdots & w_{Nq} & \cdots & u_{NN} \end{vmatrix}$$

$$C' = \det [U]$$

$$D' = \begin{vmatrix} u_{11} & \cdots & \overset{q}{w_{1q}} & \cdots & u_{1N} \\ \cdot & \cdots & \cdot & \cdots & \cdot \\ \cdot & \cdots & \cdot & \cdots & \cdot \\ u_{N1} & \cdots & w_{Nq} & \cdots & u_{NN} \end{vmatrix}.$$

Equation (12) shows that A', B', C', and D' are quantities proportional to the so-called transfer parameters A, B, C, and D of the equivalent two-port circuit. In order that the reciprocity condition ($\sqrt{AD-BC}=1$) holds, we should divide A', B', C', and D' by $\sqrt{A'D'-B'C'}$ to get A, B, C, and D, respectively, as

$$\begin{pmatrix} A & B \\ C & D \end{pmatrix} = \frac{1}{\sqrt{A'D' - B'C'}} \begin{pmatrix} A' & B' \\ C' & D' \end{pmatrix}. \tag{13}$$

When the circuit is a one-port circuit, the input admittance is given simply as (C'/A').

When the circuit has no coupling port and no circuit loss, $C'=0$ gives the proper frequency; that is, the resonant frequency of the circuit. In this situation the planar circuit is the Babinet dual of a metal wall TE-mode waveguide at its cutoff frequency.

D. Examples of Computer Analysis

In computing G_{ij} and F_{ij}, the integrals in (6) can be subdivided into as many subsections as necessary to assure the desired accuracy. However, in the following calculations the simplest approximation is used:

$$G_{ij} = \cos \theta_{ij} H_1^{(2)}(kr_{ij}) W_j \tag{14}$$

$$F_{ij} = H_0^{(2)}(kr_{ij}). \tag{15}$$

1) One-Port Disk-Shaped Circuit: As an example of the computer analysis, the input admittance of a one-port disk-shaped circuit with $\epsilon_r=2.62$, $a=1.841\,[\mathrm{m}]$, $d=0.628\,[\mathrm{m}]$ was computed first. (These values are not realistic ones; $a=1.841\,[\mathrm{m}]$ is used so that the fundamental resonant mode is given by $k=1\,[\mathrm{m}^{-1}]$.) The result is shown in Fig. 6. This figure shows the variation of the input admittance, given by (C'/A'), around the fundamental resonant frequency $f_0=1.841/2\pi a\sqrt{\epsilon\mu}$ where 1.841 is the first root of $J_1'(x)$. The parameter N denotes the number of the sampling points along the periphery.

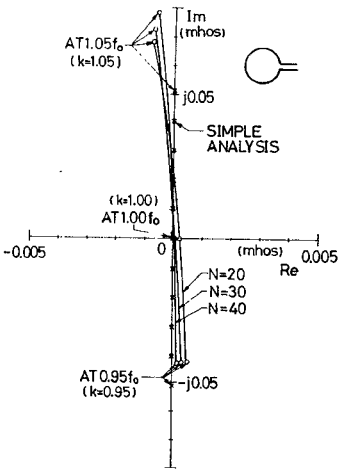

Fig. 6. Input admittance of an one-port disk-shaped circuit.

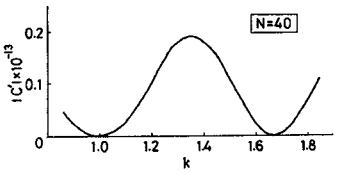

Fig. 7. The variation of $|C'|$ as a functions of k of a disk-shaped circuit.

TABLE I

COMPUTED FIRST EIGENVALUE k CORRESPONDING TO DIPOLE MODE OF A DISK-SHAPED CIRCUIT FOR VARIOUS N

Number of Sections N	Eigenvalue k
20	1.00013
30	1.00008
40	1.00007

As N increases, the real frequency locus approaches the values obtained by the simple theories as described in Section IV, shown as the small crosses along the ordinate in Fig. 6. Note that the abscissa is expanded by a factor of ten to exaggerate the computation error.

The values of k giving $C'=\det [U]=0$ corresponds to the resonant frequencies of the circuit. From the simple analyses to be described in Section IV, they should satisfy $J_m'(ka)=0$. For $a=1.841\,[\mathrm{m}]$, k should then be $1.000\,[\mathrm{m}^{-1}]$, $1.659\,[\mathrm{m}^{-1}]$, and so forth. This fact gives a good check of the computation accuracy.

Since C' is complex due to the computation error and $C'=0$ is never realized for real k, we define k which gives the minimum of $|C'|$ as the eigenvalue. The variation of $|C'|$ is shown as a function of k in Fig. 7, which shows the first ($k=1.00$) and the second ($k=1.66$) minima. The former corresponds to the fundamental dipole mode (the first root of $J_1'(ka)=0$) and the latter to the quadrupole mode (the first root of $J_2'(ka)=0$). Table I shows the former k obtained for various N. As N increases k tends toward unity.

2) Two-Port Disk-Shaped Circuit: Next the transfer parameters A, B, C, and D of a disk-shaped circuit

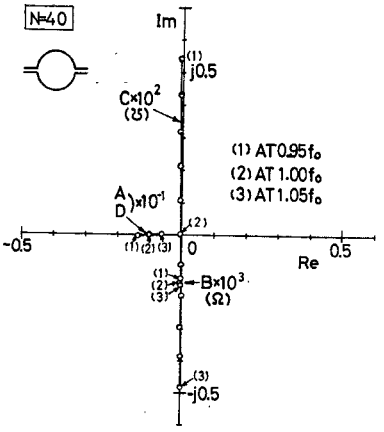

Fig. 8. Transfer parameters of a two-port disk-shaped resonator.

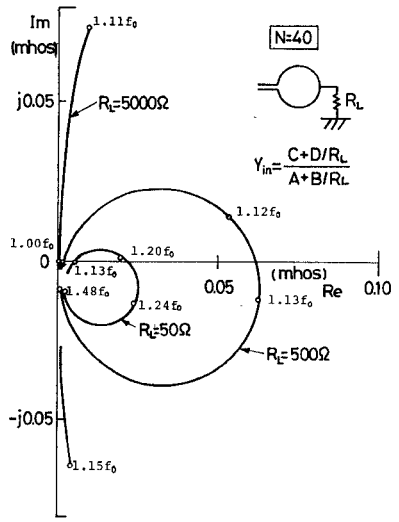

Fig. 9. Input admittance of a two-port disk-shaped resona tor loaded by various load resistances R_L.

having two-ports on its opposite sides were computed, and the result is shown in Fig. 8. In this figure the abscissa gives the real part and the ordinate the imaginary part of the transfer parameters obtained in the case $N=40$. Parameters A and D are equal to each other, as the circuit is symmetrical, and they take -1.0 at the resonant frequency.

By using the obtained transfer parameters and the relation $Y_{in}=(C+D/R_L)/(A+B/R_L)$, the input admittance of the disk-shaped circuit loaded by a pure resistance R_L was computed as shown in Fig. 9. The curves show the computer calculations for load resistances of 50, 500, and 5000 Ω. The loci in this figure cover a frequency range from the dipole mode of resonance to the quadrupole mode of resonance. In between these two low-admittance, parallel resonant points we find the frequency where the input admittance is very high, that is, a series resonant point, on the right-hand sides of loci. Note that such frequencies can never be found except by computer analysis.

Fig. 10 shows the RF voltage distribution along the

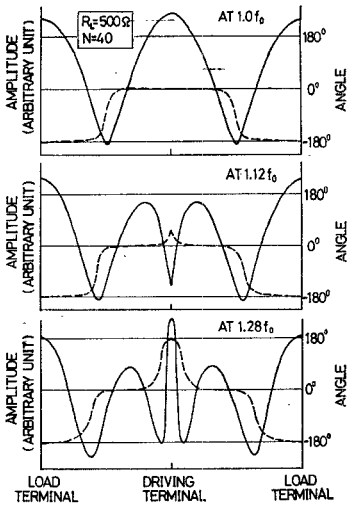

Fig. 10. The RF voltage distribution, magnitude (solid curve), and phase (broken curve), along the periphery of a disk-shaped circuit for $R_L=500$ Ω and $N=40$, for various frequencies.

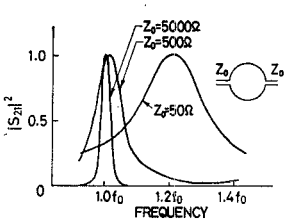

Fig. 11. The power transmission of a disk-shaped circuit calculated numerically for various characteristic impedances.

periphery for $R_L=500$ Ω and $N=40$, for various frequencies. In this figure, both ends and the center of the abscissa correspond to the load terminal and the driving terminal, respectively. The solid and broken curves show the magnitude (arbitrary scale) and phase of the RF voltage along the periphery, respectively. It is found that as the frequency increases, the distribution of the RF voltage changes from a dipole mode to a quadrupole mode. At the frequency of $1.12f_0$, the RF voltage at the input port is minimized; this corresponds to the series resonance of the circuit.

Fig. 11 shows the power transmission calculated numerically by using the relation $S_{21}=2Z_0/(AZ_0+B+CZ_0^2+DZ_0)$ for the case when the characteristic impedances Z_0 of the input and output lines are equal to each other and are pure resistance. It is found that both the frequency giving the maximum power transmission and the transmission bandwidth increase as the line impedance Z_0 is lowered.

3) Arbitrarily Shaped Circuit: As an example of more irregularly shaped circuit, a planar circuit, as shown in Fig. 12, was studied. Fig. 13 shows the frequency loci of the input admittance for $R_L=500$ Ω and $N=32$. In this figure f_0 denotes the resonant frequency of the quadrupole mode of a regular square circuit having dimensions $2a$ by $2a$. In this figure parallel resonances are found at $0.54f_0$ and $0.86f_0$, and a series resonance at $0.64f_0$.

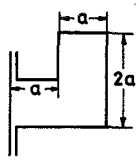

Fig. 12. Center conductor of an irregularly shaped circuit.

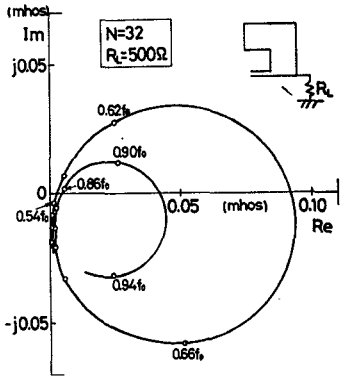

Fig. 13. The frequency locus of the input admittance for $R_L = 500\ \Omega$ and $N = 30$.

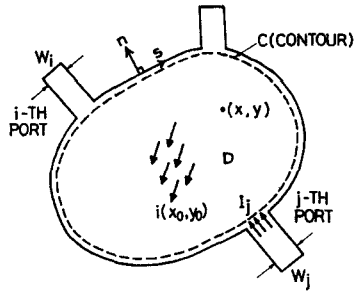

Fig. 14. Symbols used in the Green's function analysis.

IV. Analysis Based Upon Green's Function

When the shape of the circuit is relatively simple (a disk, for example) and we can get the Green's function of the wave equation analytically, the equivalent circuit parameters can be derived directly from the Green's function as follows.

We introduce the Green's function G of the second kind, having a dimension of impedance which satisfies

$$V(x, y) = \iint_D G(x, y \mid x_0, y_0) i(x_0, y_0) dx_0 dy_0 \qquad (16)$$

inside the contour C shown in Fig. 14, and an open boundary condition

$$\partial G/\partial n = 0 \qquad (17)$$

along C. In (16), $i(x_0, y_0)$ denotes an assumed (fictitious) RF current density injected normally into the circuit (see Fig. 14).

In a real planar circuit, current is injected from the periphery where a coupling port is present. Hence the RF voltage at a point upon the periphery is given by a line integral

$$V(s) = -\oint_c G(s \mid s_0) i_n(s_0) ds_0 \qquad (18)$$

where s and s_0 are used to denote distance along C, and i_n is the line current density normal to C at coupling ports. Since i_n is present only at coupling ports, the RF voltage at the ith port is given approximately as

$$V_i \doteq \sum_j I_j \frac{1}{2W_iW_j} \int_{W_i} \int_{W_j} G(s \mid s_0) ds_0 ds \qquad (19)$$

where $I_j = -2\int_{W_j} i_n(s_0) ds_0$ represents the current flowing into the jth port on both the upper and lower surfaces. Hence, the elements of the impedance matrix of the equivalent N-port circuit are

$$z_{ij} = \frac{1}{2W_iW_j} \int_{W_i} \int_{W_j} G(s \mid s_0) ds_0 ds. \qquad (20)$$

As examples of the analysis based upon Green's function, the input impedances of one port disk and square circuits as shown in Fig. 15 are calculated.

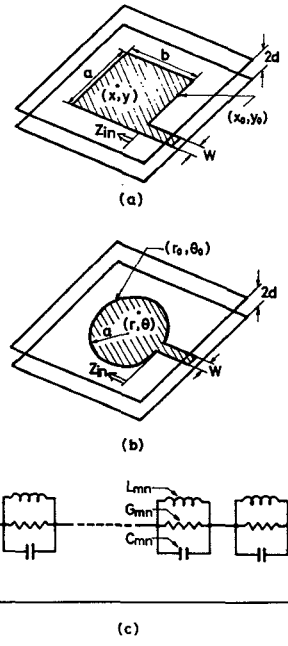

Fig. 15. (a) One-port square resonator. (b) One-port disk-shaped resonator. (c) The equivalent circuit describing the input admittance of one-port resonator.

A. Square Circuit

For a square circuit pattern [see Fig. 15(a)] having $a \times b$, the Green's function is given as [9]

$$G(x, y \mid x_0, y_0) = j\omega\mu d \frac{4}{ab} \sum_n \sum_m \frac{\cos(k_x x_0) \cos(k_y y_0)}{k_x^2 + k_y^2 - k^2} \cdot \cos(k_x x) \cos(k_y y) \qquad (21)$$

where $k_x = m\pi/a$ and $k_y = n\pi/b$.

We compute the input impedance [Z_{in} shown in Fig. 15(a)] of a one-port square circuit having the

TABLE II

THE PROPER FUNCTION AND EQUIVALENT CIRCUIT PARAMETERS OF THE TRIPLATE-TYPE, SQUARE, AND DISK CIRCUITS

Planar Resonator	Square Resonator [Fig. 15(a)]	Disk Resonator [Fig. 15(b)]
Proper function	$\cos(k_x x)\cos(k_y y)$	$J_m(k_{mn}r)\cos(m\theta)$
Resonant frequency f_{mn}	$\frac{\sqrt{(m/a)^2+(n/b)^2}}{2\sqrt{\epsilon\mu}}$	$\frac{k_{mn}}{2\pi\sqrt{\epsilon\mu}}$
C_{mn}	$\frac{\epsilon ab}{2d}\frac{1}{F}$	$\epsilon\frac{\pi a^2}{d}\{1-m^2/(ak_{mn})^2\}\frac{1}{F}$
L_{mn}	$\frac{2\mu d}{ab\{(m\pi/a)^2+(n\pi/b)^2\}}F$	$\frac{\mu d}{\pi}\frac{1}{(ak_{mn})^2-m^2}F$
G_{mn}	$2\pi f_{mn}C_{mn}/Q_0$	$2\pi f_{mn}C_{mn}/Q_0$
F	$\left(\frac{\sin(k_xW)}{k_xW}\right)^2$	$\left(\frac{\sin(mW/a)}{mW/a}\right)^2$
Q_0	$Q_0^{-1}=Q_d^{-1}+Q_c^{-1}$ $Q_d=1/\tan\delta$ (δ is the loss angle of the dielectrics) $Q_c=d/r$ (r is the skin depth of the conductor)	

coupling port at one of the corners as shown in Fig. 15(a). Equations (20) and (21) directly give

$$Z_{\text{in}} = \sum_n \sum_m \frac{j\omega\mu d(\sin(k_xW)/k_xW)^2}{ab(k_x^2 + k_y^2 - k^2)}. \tag{22}$$

When we use (F1) and (F2) to consider the circuit loss, we obtain, after some computations,

$$Z_{\text{in}} = \sum_n \sum_m \frac{1}{\left(j\omega C_{mn} - j\frac{1}{\omega L_{mn}} + G_{mn}\right)} \tag{23}$$

where C_{mn}, L_{mn}, and G_{mn} are the equivalent circuit parameters corresponding to each mode, and are tabulated in Table II.[3] Equation (23) suggests that the equivalent circuit describing the input impedance is given [see Fig. 15(c)] as a series connection of many parallel resonating circuits representing each resonance.

B. Disk Circuit

The disk circuit is shown in Fig. 15(b). The Green's function is given as

$$G(r, \theta \mid r_0, \theta_0) = \sum_n \sum_m \frac{2j\omega\mu d J_m(k_{mn}a)J_m(k_{mn}r)\cos(m(\theta-\theta_0))}{(k_{mn}^2 - k^2)a^2(1 - m^2/a^2k_{mn}^2)J_m^2(k_{mn}a)} \tag{24}$$

where k_{mn} satisfies

$$\frac{\partial}{\partial r}J_m(k_{mn}r)\Big|_{r=a} = 0 \quad (n\text{th root}). \tag{25}$$

[3] When we are concerned only with the circuit performance near a single resonant frequency, we can also derive the equivalent circuit parameters from the resonant frequency, stored energy, and the unloaded Q factor. The parameters thus obtained agree with those shown in Table II, except for the factor F describing the effect of the width of the terminal. This sort of analysis is fairly common in microwave circuit analyses. For example, one of the reviewers of this paper called the authors' attention to [10].

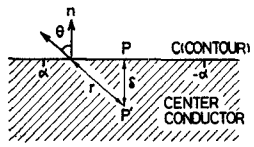

Fig. 16. Symbols used in the derivation of (4).

The equivalent circuit parameters of a one-port disk-shaped circuit can be computed by using (20), and are tabulated in Table II.

C. Multiport Disk and Square Circuits

The Green's function analysis can be applied to the circuit of this sort, which is useful in practical integrated circuitry as filters or hybrids. However, those examples are omitted for space limitations and will be reported elsewhere.

V. CONCLUSION

What is emphasized is that we can analyze an arbitrarily shaped planar circuit within a reasonable computer time. The *design* of a planar circuit, based upon the high-speed computer analysis and the trial-and-error principle, will also be possible within several years.[4]

Among possible applications of the planar circuit, the applications in Gunn and IMPATT oscillators seem to be promising. Since they are oscillation devices having relatively low impedances, the oscillator performance can be improved by using the planar circuit instead of the stripline circuitry.

APPENDIX

DERIVATION OF EQUATION (4)

The RF voltage at a piont P' *inside* the periphery satisfies the following Weber's solution for cylindrical waves [6],

$$4jV(P') = \oint_c \left\{H_0^{(2)}(kr)\frac{\partial V(Q)}{\partial n} - V(Q)\frac{\partial H_0^{(2)}(kr)}{\partial n}\right\} ds. \tag{A1}$$

To obtain the RF voltage of the point P just *upon* the periphery, a little algebra is required. We first define a point P' just inside the point P as shown in Fig. 16, where we assume that $\delta \ll \alpha \ll k^{-1}$. By using the following approximations of the Hankel function near the origin

$$H_0^{(2)}(kr) \fallingdotseq -\frac{2j}{\pi}\log\frac{k\sqrt{s^2+\delta^2}}{2}$$

$$\frac{\partial H_0^{(2)}(kr)}{\partial n} \fallingdotseq -\frac{2j}{\pi}\frac{\delta}{s^2+\delta^2}$$

[4] For example, the time required to obtain the entire data in Fig. 8 is about 100 s using a typical Japanese high-speed computer HITAC-5020E. The improvement in the speed by a factor of (1/10) may be needed for the design.

we can rewrite

$$4jV(P') = \int_{-\alpha}^{\alpha} \left\{ -\frac{2j}{\pi} \log \frac{k\sqrt{s^2+\delta^2}}{2} \frac{\partial V}{\partial n} + \frac{2j}{\pi} \frac{\delta}{s^2+\delta^2} V \right\} ds + \int_{\Gamma} \left\{ H_0^{(2)}(kr) \frac{\partial V}{\partial n} - V \frac{\partial H_0^{(2)}(kr)}{\partial n} \right\} ds \quad \text{(A2)}$$

where Γ denotes the contour excluding the section $-\alpha \sim +\alpha$. If V and $\partial V/\partial n$ vary slowly in the minute section between $-\alpha$ and α, the integrals in (A2) become

$$-\frac{2j}{\pi} \int_{-\alpha}^{\alpha} \log \frac{k\sqrt{s^2+\delta^2}}{2} \frac{\partial V}{\partial n} ds = -\frac{4j}{\pi} \frac{\partial V}{\partial n} \left\{ \alpha \left(\log \frac{k\sqrt{\alpha^2+\delta^2}}{2} - 1 \right) - \frac{k\delta}{2} \left(\operatorname{arc\,cosec} \frac{\sqrt{\alpha^2+\delta^2}}{\delta} - \frac{\pi}{2} \right) \right\} \quad \text{(A3)}$$

$$\frac{2j}{\pi} \int_{-\alpha}^{\alpha} \frac{s}{s^2+\delta^2} V ds = \frac{2j}{\pi} V \tan^{-1} \frac{\alpha}{\delta}. \quad \text{(A4)}$$

When P' approaches P, and hence δ tends to zero, (A2), (A3), (A4) give

$$4jV(P') = -\frac{4j}{\pi} \frac{\partial V}{\partial n} \left\{ \alpha \left(\log \frac{k\alpha}{2} - 1 \right) \right\} + 2jV(P) + \int_{\Gamma} \left\{ H_0^{(2)}(kr) \frac{\partial V}{\partial n} - V \frac{\partial H_0^{(2)}(kr)}{\partial n} \right\} ds. \quad \text{(A5)}$$

Next, as α tends to zero, the first term in the right-hand side of (A5) vanishes, and hence

$$2jV(P) = \oint_c \left\{ H_0^{(2)}(kr) \frac{\partial V}{\partial n} - V \frac{\partial H_0^{(2)}(kr)}{\partial n} \right\} ds. \quad \text{(A6)}$$

This equation and the relations

$$\frac{\partial V}{\partial n} = -j\omega\mu d\, i_n$$

$$\frac{\partial H_0^{(2)}(kr)}{\partial n} = -k \cos\theta H_1^{(2)}(kr)$$

give (4) in the text.

Acknowledgment

The authors wish to thank M. Hashimoto of Osaka University, Osaka, Japan, for stimulating discussions.

References

[1] T. Okoshi, "The planar circuit," in *Rec. of Professional Groups, IECEJ*, Paper SSD68-37/CT68-47, Feb. 17, 1969.
[2] ——, "The planar circuit," *J. IECEJ*, vol. 52, no. 11, pp. 1430–1433, Nov. 1969.
[3] S. Mao, S. Jones, and G. D. Vendelin, "Millimeter-wave integrated circuits," *IEEE Trans. Microwave Theory Tech. (Special Issue on Microwave Integrated Circuits)*, vol. MTT-16, pp. 455–461, July 1968.
[4] Y. Tajima and I. Kuru, "An integrated Gunn oscillator," in *Rec. of Professional Groups, IECEJ*, Paper MW70-9, June 26, 1970.
[5] H. Bosma, "On stripline Y-circulation at UHF," *IEEE Trans. Microwave Theory Tech. (1963 Symposium Issue)*, vol. MTT-12, pp. 61–72, Jan. 1964.
[6] J. A. Stratton, *Electromagnetic Theory*. New York: McGraw-Hill, 1941, p. 460.
[7] T. Okoshi and T. Miyoshi, "The planar circuit—An approach to microwave IC," in *Proc. 1971 European Microwave Conf.*, Paper C4, Aug. 1971.
[8] —— "The planar circuit—A novel approach to microwave circuitry," in *Proc. Kyoto Int. Conf. on Circuit and System Theory*, Paper B-5-1, Sept. 1970.
[9] P. M. Morse and H. Feshbach, *Method of Theoretical Physics*, pt. II. New York: McGraw-Hill, 1953, p. 1360.
[10] S. B. Cohn, P. M. Sherk, J. K. Shimizu, and E. M. T. Jones, "Final report on strip transmission lines and components," Stanford Res. Institute, Contract DA36-0393SC-63232, Final Rep., pp. 79–162.